Clinical & Translational Immunology

Australian and New Zealand Society for Immunology Inc.

*Clinical & Translational Immunology* 2021; e1245. doi: 10.1002/cti2.1245
www.wileyonlinelibrary.com/journal/cti

ORIGINAL ARTICLE

# Pattern of circulating SARS-CoV-2-specific antibody-secreting and memory B-cell generation in patients with acute COVID-19

Maria Byazrova[1,2], Gaukhar Yusubalieva[3], Anna Spiridonova[1], Grigory Efimov[4], Dmitriy Mazurov[5], Konstantin Baranov[6], Vladimir Baklaushev[3] & Alexander Filatov[1,2]

[1]National Research Center Institute of Immunology of Federal Medical Biological Agency of Russia, Moscow, Russia
[2]Department of Immunology, Faculty of Biology, Lomonosov Moscow State University, Moscow, Russia
[3]Federal Research and Clinical Center for Specialized Types of Medical Care and Medical Technologies of the FMBA of Russia, Moscow, Russia
[4]National Research Center for Hematology, Moscow, Russia
[5]Institute of Gene Biology Russian Academy of Sciences, Center for Precision Genome Editing and Genetic Technologies for Biomedicine, Moscow, Russia
[6]Institute of Molecular and Cellular Biology SB RAS, Lomonosov Moscow State University, Novosibirsk, Russia

**Correspondence**
A Filatov, National Research Center Institute of Immunology of Federal Medical Biological Agency of Russia, Moscow, Russia.
Email: avfilat@yandex.ru

Received 28 October 2020;
Revised 7 January 2021;
Accepted 7 January 2021

doi: 10.1002/cti2.1245

*Clinical & Translational Immunology*
2021; **10**: e1245

## Abstract

**Objectives.** To predict the spread of coronavirus disease (COVID-19), information regarding the immunological memory for disease-specific antigens is necessary. The possibility of reinfection, as well as the efficacy of vaccines for COVID-19 that are currently under development, will largely depend on the quality and longevity of immunological memory in patients. To elucidate the process of humoral immunity development, we analysed the generation of plasmablasts and virus receptor-binding domain (RBD)-specific memory B (Bmem) cells in patients during the acute phase of COVID-19. **Methods.** The frequencies of RBD-binding plasmablasts and RBD-specific antibody-secreting cells (ASCs) in the peripheral blood samples collected from patients with COVID-19 were measured using flow cytometry and the ELISpot assay. **Results.** The acute phase of COVID-19 was characterised by the transient appearance of total as well as RBD-binding plasmablasts. ELISpot analysis indicated that most patients exhibited a spontaneous secretion of RBD-specific ASCs in the circulation with good correlation between the IgG and IgM subsets. IL-21/CD40L stimulation of purified B cells induced the activation and proliferation of Bmem cells, which led to the generation of plasmablast phenotypic cells as well as RBD-specific ASCs. No correlation was observed between the frequency of Bmem cell-derived and spontaneous ASCs, suggesting that the two types of ASCs were weakly associated with each other. **Conclusion.** Our findings reveal that SARS-CoV-2-specific Bmem cells are generated during the acute phase of COVID-19. These findings can serve as a basis for further studies on the longevity of SARS-CoV-2-specific B-cell memory.

**Keywords:** antibody-secreting cell, memory B cell, plasmablast, SARS-CoV-2, virus-neutralising antibodies

## INTRODUCTION

The pathogenesis of coronavirus disease (COVID-19), which has been declared a global pandemic, is inextricably linked to the immune response to SARS-CoV-2.[1] All three branches of immunity are involved in providing protection against the pathogen. At present, humoral immune response including the production of SARS-CoV-2-specific and virus-neutralising antibodies is the most studied topic related to immunity against COVID-19.[2]

There is significant interest regarding antibodies that target the receptor-binding domain (RBD) of the coronavirus surface spike protein, which binds to the target cell by interacting with the entry receptor, the human angiotensin-converting enzyme 2 (ACE2).[3] After binding, the spike protein promotes the entry of the virus into the target cell. The level of RBD-specific antibodies in most patients with COVID-19 exhibits a good correlation with the activity of SARS-CoV-2-neutralising antibodies. This indicates that the RBD is the primary target of SARS-CoV-2-neutralising antibodies,[4–6] thereby suggesting the crucial role of RBD-specific antibodies in infection control. Therefore, the induction of an RBD-specific B-cell response represents an important aspect of immunity against SARS-CoV-2.

The prognosis for the further spread of COVID-19 depends on the proportion of recovered patients who are able to acquire a stable immunological memory against SARS-CoV-2 antigens. The quality of the immunological memory will also influence the efficacy of future vaccines for COVID-19. Owing to its recent emergence, COVID-19 has a considerably short history of research. Therefore, long-term predictions for SARS-CoV-2 immunological memory are primarily based on the data currently available for SARS-CoV and other coronaviruses.[7] It has been reported that the level of SARS-CoV-specific IgG peaks during the fourth month, following which it is maintained at a significant level for more than 2 years,[8] after which it gradually declines and tends to reach the baseline level 5–6 years post-disease onset.[9] SARS-CoV-specific memory T-cell response can be detected even after 17 years of infection.[10] In contrast, SARS-CoV B-cell memory may not be as long lasting. In a case study on two patients who had recovered from SARS-CoV infection, memory B (Bmem) cells could be detected at 3 months post-infection; however, the frequencies were considerably low at 3.5 years after recovery.[9] Information on SARS-CoV-2-specific B-cell memory is considerably limited. Bmem cells obtained from recently recovered patients have been actively used for the isolation and sequencing of immunoglobulin (Ig) genes for the subsequent generation of SARS-CoV-2-neutralising antibodies.[4,5,11,12] However, Bmem cells *per se*, and their generation and action dynamics are yet to be studied extensively.

In recent studies, Bmem cells have been detected as cells binding fluorescently labelled SARS-CoV-2 antigens, and the kinetics of Bmem cell response has been analysed over 6 months.[13,14] These studies were mainly performed with SARS-CoV-2 convalescent donors, when Bmem cells are already formed and present in quantities available for determination by flow cytometry. Herein, we aimed to study the generation of the Bmem cell response during the acute phase of SARS-CoV-2 infection. Since Bmem cells begin to appear and are rather rare in the acute phase, we used the highly sensitive ELISpot assay. In addition, we compared Bmem cell response with the plasmablast and serum IgG responses. The use of the virus neutralisation test allowed us not only to detect Bmem cells, but also to assess their functional activity.

## RESULTS

We aimed to evaluate the B-cell response to SARS-CoV-2 infection. The study group included 42 patients with the moderate form and 30 patients with the severe form of COVID-19, having a mean age of 63 years. Ten age-matched healthy donors (HDs) were also included. The demographic and clinical characteristics of the cases are summarised in Supplementary tables 1 and 2. The overall study design is illustrated in Supplementary figure 1.

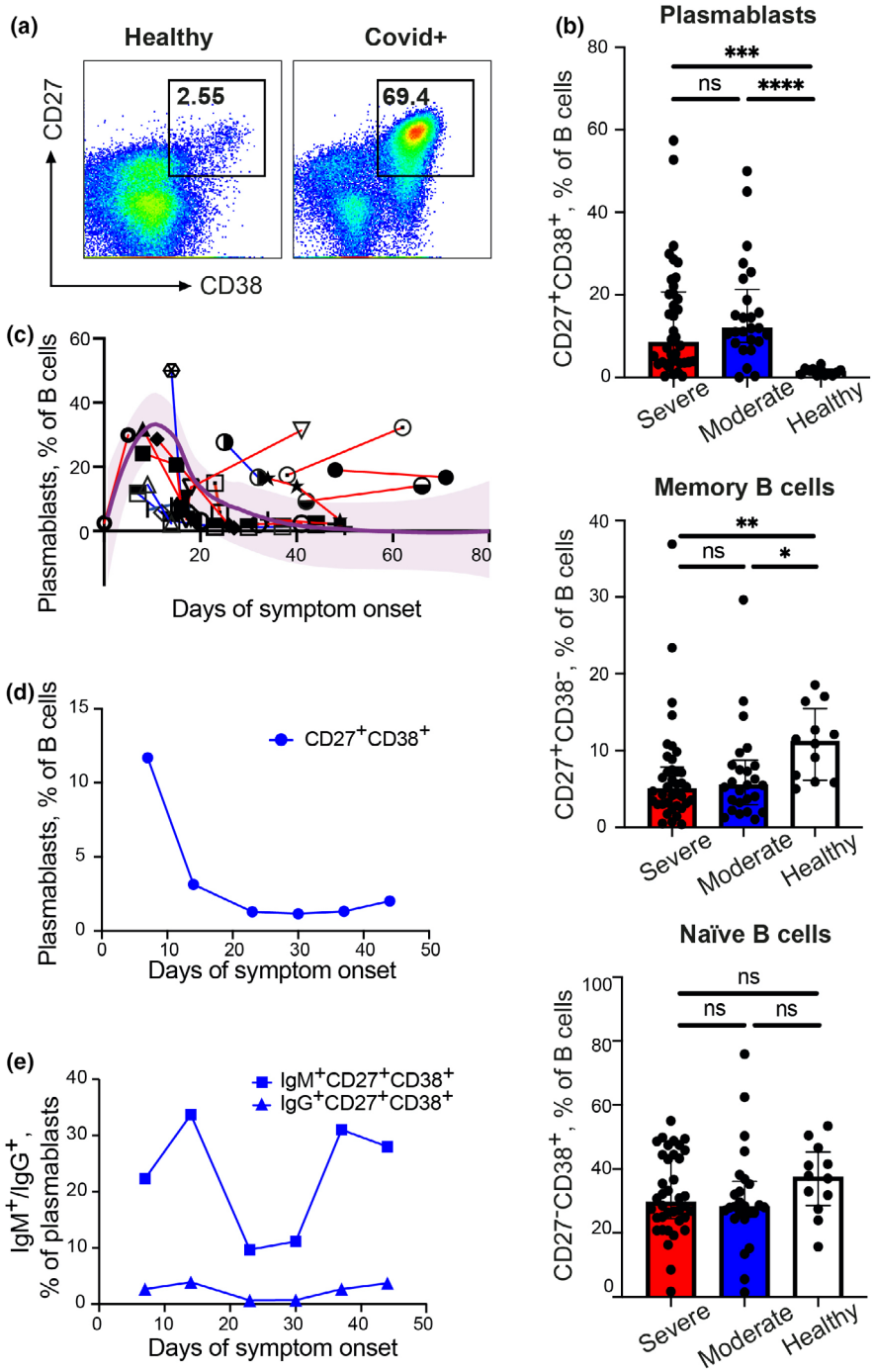


**Figure 1.** Increased plasmablast frequency in patients with COVID-19. **(a)** Flow cytometry dot plots showing plasmablast detection in a representative HD (left) and patient with severe COVID-19 (right). Numbers inside the plots indicate the percentage of events specific to respective gates; $10^6$ B-cell events were acquired for each plot. **(b)** Plasmablast (left), memory B-cell (middle) and naïve B-cell (right) frequencies within the total $CD19^+$ population in samples collected from HDs and patients with severe and moderate COVID-19. **(c)** Dynamic changes in plasmablast frequencies in samples collected from 16 patients based on the number of days after symptom onset. Symbols connected by solid lines represent two to four time points considered for each patient. LOESS-smoothed line and 95% confidence intervals are shown for 10 patients. (d, e) Longitudinal analysis of total **(d)** or $IgM^+/IgG^+$ **(e)** plasmablast response in a patient with moderate COVID-19 (P24). Results are shown for individual samples (symbols) from HDs (n = 12), and moderate (n = 25) and severe (n = 38) COVID-19 cases. Data are presented as median ± IQR. Asterisks indicate significant difference between groups determined using the Kruskal–Wallis test, $*P < 0.05$, $**P < 0.01$, $***P < 0.001$, $****P < 0.0001$, ns = not significant. HD, healthy donor; IQR, interquartile range.

## Increase in plasmablast frequency in patients with acute COVID-19

Fresh peripheral blood samples collected from the 72 patients were immunophenotyped. Flow cytometric analysis revealed that the frequencies of total $CD19^+$ B cells did not change significantly in patients compared with those in HDs (Supplementary figure 2). Concurrently, significant perturbations were observed in specific B-cell subpopulations.

We could clearly detect plasmablasts ($CD27^{hi}CD38^{hi}$) in patients with COVID-19, whereas they were practically absent in HDs (Figure 1a). In 26.4% of cases ($n = 19$), a massive induction of plasmablasts was observed, with the proportion of the subpopulation exceeding 20% of the total B-cell population. Overall, the proportion of plasmablasts was significantly higher in patients than in HDs (severe vs. HD, $P = 0.0002$; moderate vs. HD, $P < 0.0001$; Figure 1b, left panel). We observed a reduction in the proportion of Bmem cells ($CD27^+CD38^-$) in patients compared with that in HDs (severe vs. HD, $P = 0.0058$; moderate vs. HD, $P = 0.016$; Figure 1b, middle panel), which probably resulted from an increase in the proportion of plasmablasts. There was no significant difference in the percentage of naïve B cells ($CD19^+CD27^-$) between the two groups (Figure 1b, right panel).

Our study did not specifically focus on a detailed investigation of the plasmablast kinetics. However, the analysis of the samples collected from patients at different time points after disease onset provided indirect information regarding the dynamics of the plasmablast response (Figure 1c). The highest proportion of plasmablasts was observed in samples collected within the first 20 days after disease onset, following which the proportion declined to baseline levels. Concurrently, in patients who exhibited signs of acute infection for a considerably long period and continued to undergo treatment in the intensive care unit, a significant proportion of plasmablasts (from 10 to 25% of the total B-cell population) were noted even after 2 months of disease onset.

A detailed longitudinal study was performed on a patient with the moderate form of the disease (P24). The maximum plasmablast frequency was observed at 7 days after the onset of symptoms following which, it gradually decreased and approached baseline levels by day 23 (Figure 1d). The plasmablasts were primarily of the $IgM^+$ isotype; however, a small proportion of $IgG^+$ plasmablasts were also detected (Figure 1e).

## RBD-binding B-cell induction in patients with acute COVID-19

To determine whether SARS-CoV-2 infection induced the activation and expansion of coronavirus-specific B cells, we measured the frequency of RBD-binding B cells using phycoerythrin- and allophycocyanin-labelled RBD (RBD-PE and RBD-APC, respectively). RBD-binding B cells were clearly detected in the plasmablast ($CD19^+CD27^{hi}CD38^{hi}$) population, whereas they were not detected in the naïve B-cell ($CD19^+CD27^-$) population (Figure 2a). RBD-specific lymphocytes were also detected in the Bmem cell ($CD19^+CD27^+$) population; however, these cells were not stained as distinctly as that observed in the plasmablast subset. In the subsequent experiments, we performed detailed analyses using only RBD-binding plasmablasts.

In 19 patients, we detected a well-separated $RBD^+$ population (Figure 2b, top panel). RBD-PE staining was antigen-specific, as no more than 2% of the cells could bind to an irrelevant protein Betv1-PE. However, in some patients ($n = 35$), the $RBD^+$ cells exhibited a lower signal-to-noise ratio (Figure 2b, bottom panel). We used the difference between the RBD-PE and Betv1-PE samples to quantify RBD-binding B cells. As described earlier,[15,16] the quantity of antigen bound to the B-cell receptor (BCR) indicates the affinity of the corresponding BCR.

The frequencies of RBD-binding plasmablasts varied widely, and values as high as 38% of the total plasmablast population were recorded in some cases, with median values of 4.18% and an interquartile range (IQR) of 1.16–6.29 in severe cases and 4.33% (median) and 1.23–13.62 (IQR) in moderate cases (Figure 2c). This indicated that acute SARS-CoV-2 infection could significantly boost RBD-specific B-cell production. The percentage of RBD-binding cells in HDs did not exceed baseline levels.

In the sample obtained from patient P24, who was subjected to the longitudinal study, it was shown that the kinetics of RBD-specific B cells (Figure 2d) were delayed relative to the dynamics of total plasmablasts (Figure 1d), and the peak RBD-specific plasmablast frequency was observed approximately at day 23 after the onset of

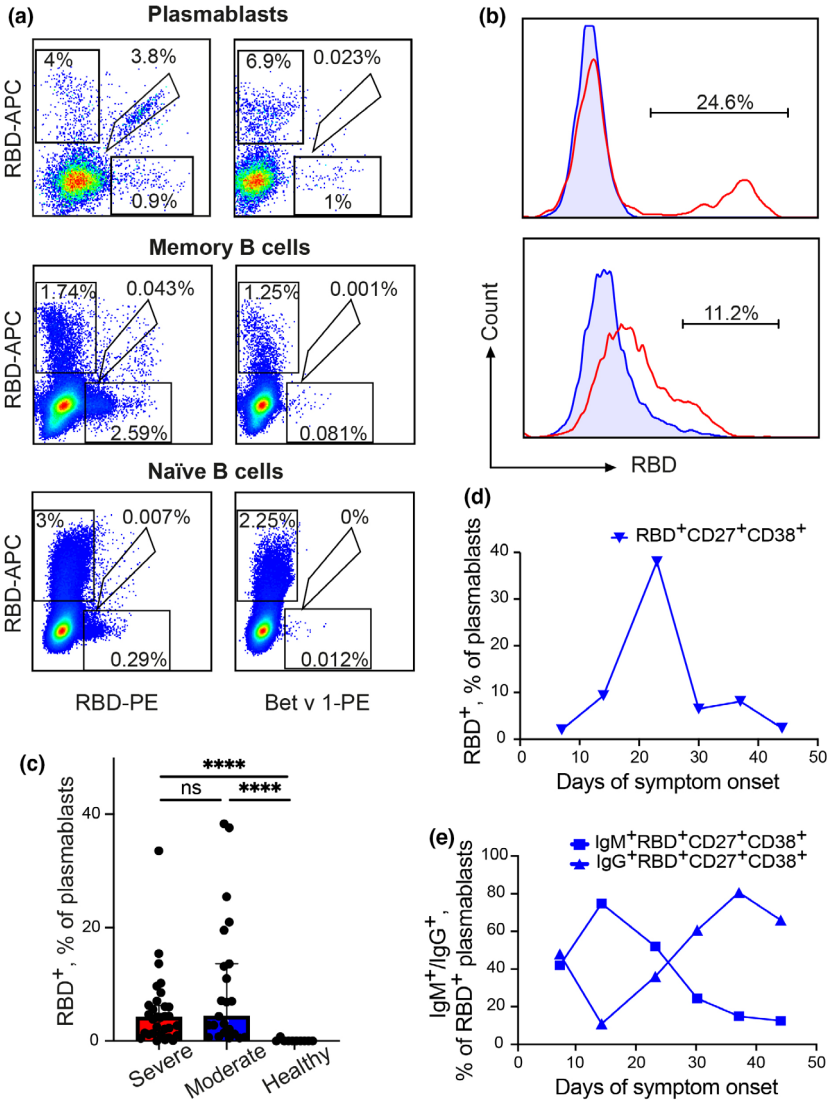


**Figure 2.** Quantification of RBD-specific B cells in fresh blood samples collected from patients with COVID-19. **(a)** Representative flow cytometry dot plots showing double discrimination of $RBD^+$ cells in plasmablast (top row), memory B-cell (middle row) and naïve B-cell (bottom row) subsets. Plasmablasts, memory B cells and naïve B cells were gated as $CD27^+CD38^+$, $CD27^+CD38^-$ and $CD27^-$, respectively; 800 000 B-cell events were acquired for each plot. **(b)** Representative bimodal (top panel) or unimodal (bottom panel) phycoerythrin-labelled RBD staining histograms. For comparison, binding to the irrelevant protein Betv1-PE is shown. **(c)** $RBD^+$ frequencies within plasmablast population from HDs and patients with moderate (n = 22) and severe (n = 31) COVID-19. (d, e) Dynamic changes in total **(d)** or $IgM^+/IgG^+$ **(e)** RBD-specific plasmablast populations in sample obtained from P24 (patient with moderate COVID-19). Results are shown for individual samples (symbols) from HDs (n = 12), and moderate (n = 25) and severe (n = 38) COVID-19 cases. Data are presented as median ± IQR. Asterisks indicate significant difference between groups determined using the Kruskal–Wallis test, $^{****}P < 0.0001$, ns = not significant. HD, healthy donor; IQR, interquartile range; RBD, receptor-binding domain.

symptoms. Initially, the $RBD^+$ plasmablasts were primarily of the $IgM^+$ type, whereas later, the $IgG^+$ type was detected predominantly (Figure 2e). These findings are in good agreement with the classical scheme, according to which the primary response is primarily mediated by $IgM^+$ B cells, while the secondary response is mediated by $IgG^+$ B cells. We suggest that the brightly stained $RBD^+$ plasmablasts corresponded to the early plasmablasts that retained the BCR.[17] Despite the fact that in some cases the determination of RBD-binding B cells is quite straightforward, it may have some difficulties in general. Therefore, RBD-specific B cells were further explored by

measuring antibody-secreting cells (ASCs) using an ELISpot assay.

## Response of circulating RBD-specific ASCs in patients with COVID-19

Next, 24 individuals from the study group were selected at random and subjected to further detailed analyses. RBD-specific and total Ig ASCs isolated from fresh blood samples were analysed using the ELISpot assay. The demographic, clinical, and virological characteristics of these cases, the status of illness, and the time points of sampling are summarised in a swimmer plot (Supplementary figure 3).

Plasmablasts are the primary ASCs present in the blood. To test this, plasmablasts ($CD19^{+}CD27^{hi}CD38^{hi}$) and Bmem cells ($CD19^{+}CD27^{+}CD38^{-}$) were sorted using flow cytometry, and their ability to secrete RBD-specific antibodies was analysed using the ELISpot assay. As shown in Supplementary figure 4, numerous total IgG or IgM ASCs, along with RBD-specific ASCs, were detected in the plasmablast population. In contrast, the unstimulated Bmem cells produced neither IgG nor IgM antibodies. Therefore, in the blood samples, the circulating ASCs were a part of the plasmablast population and not a part of the Bmem cell population. To avoid subjecting the cells to unnecessary manipulations in subsequent experiments for the measurement of ASC abundance in fresh blood samples, we used the total population of peripheral blood mononuclear cells (PBMCs), with the results obtained being attributed to plasmablasts.

PBMCs isolated from samples obtained from 15 patients with COVID-19 were assessed for total Ig and RBD-specific ASC responses. Of note, spots corresponding to IgG-secreting cells were generally larger than those corresponding to IgM-secreting cells (Figure 3a), which probably reflects the difference in Ig secretion rates.[18,19] The ELISpot analysis indicated that patients had positive RBD-specific ASC responses, with a median frequency of 170 IgM ASCs per $10^6$ PBMCs (IQR, 8–1144) and 314 IgG ASCs per $10^6$ PBMCs (IQR, 103–1320). To calculate the frequency of antigen-specific ASCs in the total B-cell population, the number of RBD-specific IgM or IgG ASCs was divided by the total number of IgM or IgG ASCs. As indicated by the B-cell ELISpot assay, the percentage of RBD-specific IgM and IgG ASCs ranged from 0.14 to 80% of the total number of Ig ASCs (Supplementary figure 5).

To compare the responses of IgG and IgM ASCs, Spearman's rank correlation analysis was performed. A strong correlation was observed between the frequencies of RBD-specific IgG and IgM ASCs (Spearman's $r = 0.95$, $P < 0.0001$) (Figure 3c). Considering the results of the ELISpot assay for the HD group, the threshold for a positive RBD-specific ASC response was established as 20 spot-forming cells per $10^6$ input cells. In two cases (P20 and P22), both IgG and IgM ASC responses were below the baseline levels of ASCs observed in the HD group. These patients could be considered non-responders (Figure 3c). We observed two more cases with negative IgM and considerably weak IgG responses. These patients could be considered low responders as well. We did not observe a correlation between the frequency of $RBD^{+}$ plasmablasts and RBD-specific IgG/IgM ASCs (Figure 3d). Samples with the highest RBD-specific IgM or IgG ASC response only had a small proportion of RBD-binding plasmablasts, and vice versa. This could be attributed to the presence of early and late plasmablasts, the former predominantly having surface Ig and the latter having cytoplasmic/secreted Ig.[20] There was also no significant correlation between circulating RBD-specific ASCs and plasma RBD-specific Ig (Figure 3e), which is consistent with no association being found between plasma RBD IgG and plasmablasts.[2] This could have resulted from the narrow temporal peak of circulating ASCs, as well as the high dependence of the detection levels on the sampling time.

## Evidence of RBD-specific Bmem cell response

Since we studied the levels of $RBD^{+}$ plasmablasts and ASCs, the next step was to check whether Bmem cells were formed in the acute phase of SARS-CoV-2 infection. To this end, B cells were purified from PBMCs collected from 24 patients with COVID-19 using immunomagnetic cell separation. To facilitate the differentiation of Bmem cells into ASCs, purified B lymphocytes were stimulated using A549-CD40L feeder cells in the presence of 25 ng $mL^{-1}$ IL-21 for 7 days as previously described by Kwakkenboss et al.[19]

IL-21/CD40L stimulation led to the expansion of B cells (Figure 4a). In HD samples, the number of B cells increased by 10 times on an average (median expansion factor, 10.66; IQR, 4.27–14.99),

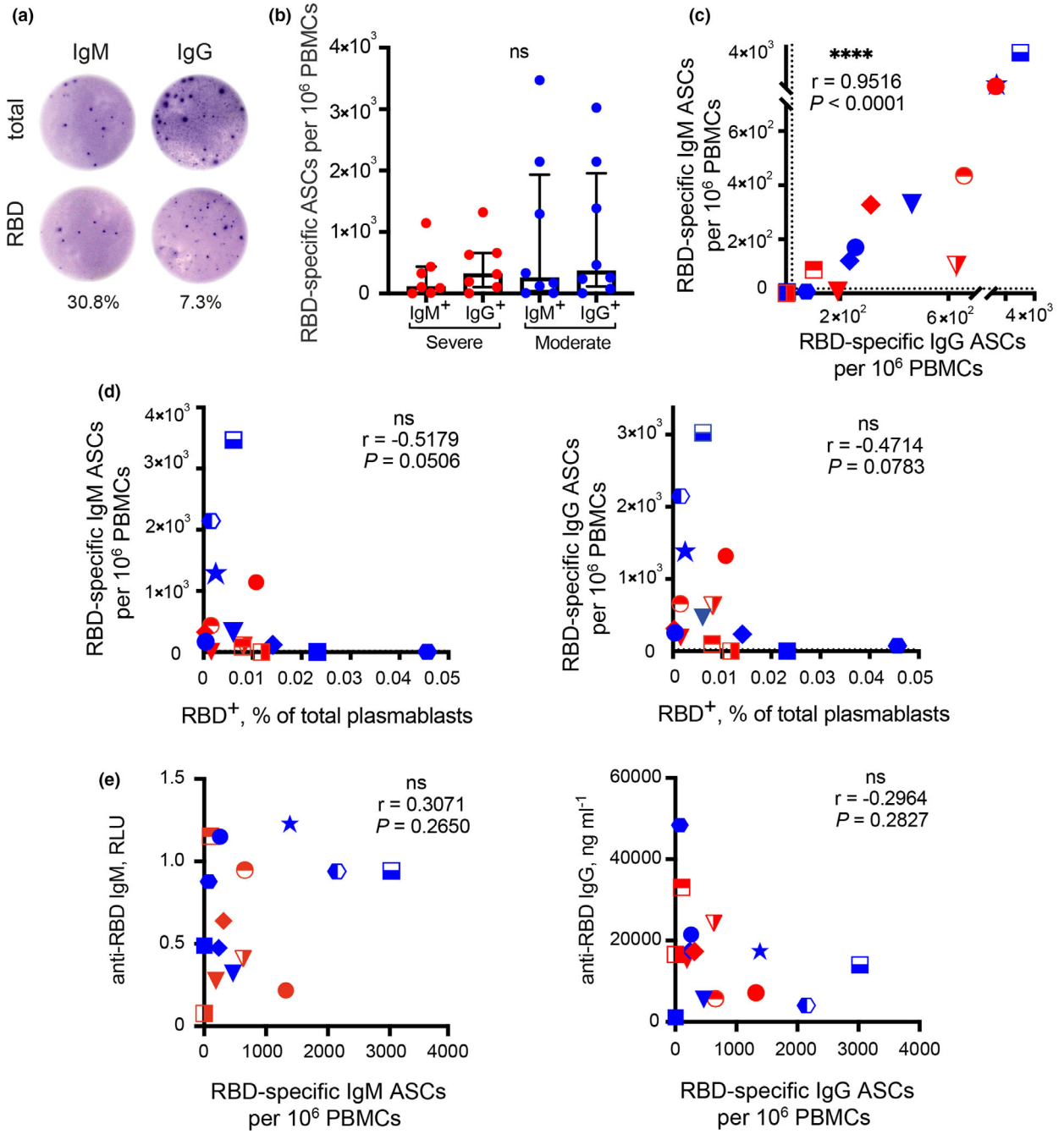


**Figure 3.** ELISpot assay of circulating ASCs. **(a)** Representative ELISpot showing RBD-specific circulating ASCs. Fresh PBMCs were incubated on ELISpot plates for 16 h to detect cells secreting total (top row) or RBD-specific (bottom row) IgMs (left column) or IgGs (right column). The wells shown contained $10^4$ PBMCs obtained from patients with COVID-19. The percentages indicated beside the wells represent the frequencies of antigen-specific ASCs relative to the total number of IgMs or IgGs. **(b)** RBD-specific ASCs per $10^6$ PBMCs collected from patients with severe (n = 7) and moderate (n = 8) COVID-19. The dotted lines indicate the threshold for a positive RBD-specific ASC response (20 spots per $10^6$ PBMCs). **(c)** Scatter plot of IgM vs. IgG RBD-specific ASCs. The dotted lines indicate the threshold for a positive RBD-specific ASC response (20 spots per $10^6$ PBMCs). **(d)** Frequencies of circulating $RBD^+$ plasmablasts (percentage of total PBMCs) determined using flow cytometry, and RBD-specific ASC IgMs (left panel) or IgGs (right panel) determined using the ELISpot assay. **(e)** Frequencies of circulating RBD-specific ASC IgMs (left panel) or IgGs (right panel) determined using the ELISpot assay, and the levels of plasma RBD-specific IgM (left panel) or IgG (right panel) determined using the ELISA. Data are presented as median ± IQR. ASC, antibody-secreting cell; HD, healthy donor; PBMC, peripheral blood mononuclear cell; IQR, interquartile range; RBD, receptor-binding domain.

which corresponded to approximately one cell division every 1.7 days. Although we did not observe a difference in fold expansion between the severe disease ($n = 13$) and HD groups, a noticeable increase was noted in the stimulation index in the moderate group (median, 10.66; IQR, 4.268–14.99; $n = 11$).

We next examined the phenotypic changes in IL-21/CD40L-stimulated B cells using flow cytometry. As noted above, the population of freshly purified PBMCs contained a large number of plasmablasts (Figure 4b, left panel). After negative magnetic separation, the purified B-cell population was completely devoid of plasmablasts (Figure 4b, middle panel). During IL-21/CD40L stimulation for 7 days, B cells with a plasmablast phenotype ($CD19^+CD20^{low\text{-}neg}CD27^+CD38^+$) were regenerated, as shown in the representative plot for a single sample (Figure 4b, right panel). The population of stimulated B lymphocytes in samples obtained from patients with COVID-19 had a low $CD27^+CD38^+$ cell frequency compared with that derived from HDs ($P = 0.0023$) (median percentage of $CD27^+CD38^+$ cells in total stimulated B cells: 14.7% in severe group, 3.7% in moderate disease group, and 27.0% in HD group; Figure 4c).

The stimulated B cells were also tested for direct binding with RBD-PE. A representative flow cytometry plot of $RBD^+$ stimulated B cells is presented in Figure 4d. The median values of $RBD^+$ stimulated B cells were 9.27% and 6.52% in the severe and moderate disease groups, respectively (severe n = 13, moderate $n = 7$; $P$ (severe vs. healthy) = 0.0011, $P$ (moderate vs. healthy) = 0.015; Figure 4e). Collectively, these data demonstrated that IL-21/CD40L stimulation for 7 days induced the proliferation and differentiation of B cells into plasmablasts.

The capacity of functional Bmem cells to differentiate into RBD-specific ASCs after IL-21/CD40L stimulation was further demonstrated using the ELISpot analysis (Figure 4f). We observed comparable frequencies of RBD-specific Bmem cell-derived IgG or IgM ASCs in both moderate and severe disease groups (Figure 4g). The median RBD-specific Bmem cell frequency ranged from 2.2 to 13.3% of total Ig-producing Bmem cells, with minimal reactivity observed in uninfected individuals. With the exception of two cases (P21 and P23), there was good correlation between RBD-specific Bmem cell-derived IgG and IgM ASCs (Spearman's $r = 0.79$, $P < 0.0001$; Figure 4h). In contrast, in case of P21 (patient with severe disease), a predominant IgM ASC response was observed, whereas in case of P23 (patient with moderate disease), a high IgG ASC response was observed and modest levels of IgM ASCs were maintained. Five cases from the study group showed considerably low yet clearly positive frequencies of both IgM and IgG ASCs. These patients could be considered low responders (Figure 4g). Interestingly, this group did not include samples that lacked circulating ASCs (Figure 3c).

To compare the plasmablast and Bmem cell responses, we performed a correlation analysis between the frequencies of spontaneous and Bmem cell-derived ASCs. Spearman's correlation analysis showed that there was no association between the IgM and IgG responses (Spearman's $r = -0.35$, $P = 0.20$ for IgM; $r = -0.42$, $P = 0.12$ for IgG; Figure 4i). This indicated that plasmablast dynamics did not correspond to the kinetics of Bmem cell generation (Supplementary figure 6).

## Production of RBD-binding and virus-neutralising antibodies induced by *in vitro* IL-21/CD40L stimulation of Bmem cells

The standard application of the ELISpot assay does not allow evaluation of the levels of secreted antibodies. To this end, the concentration of secreted IgM or IgG in the culture supernatants of IL-21/CD40L-stimulated B cells was quantified using ELISA plates coated with recombinant RBD. Total IgG secretion was observed in B cells obtained from almost all patients (Supplementary figure 7); however, supernatants from only 3 (derived from patients P5, P6 and P21) of the 23 samples showed strong reactivity in the RBD-binding test (Figure 5a). The concentration of RBD-specific IgG in these samples detected by ELISA ranged from 30 to 39 ng $mL^{-1}$. The supernatant derived from patient P5 additionally demonstrated strong RBD-specific IgA binding (Figure 5b). Moreover, the supernatant from only one sample (obtained from patient P2) showed high RBD-specific IgM activity (Figure 5c).

Along with the synthesis of RBD-specific antibodies, significant importance is also given to the secretion of functional virus-neutralising antibodies. The supernatants from the cultures of stimulated B cells were further analysed in a neutralisation assay using HIV-1-based virions pseudotyped with spike proteins of SARS-CoV-2.

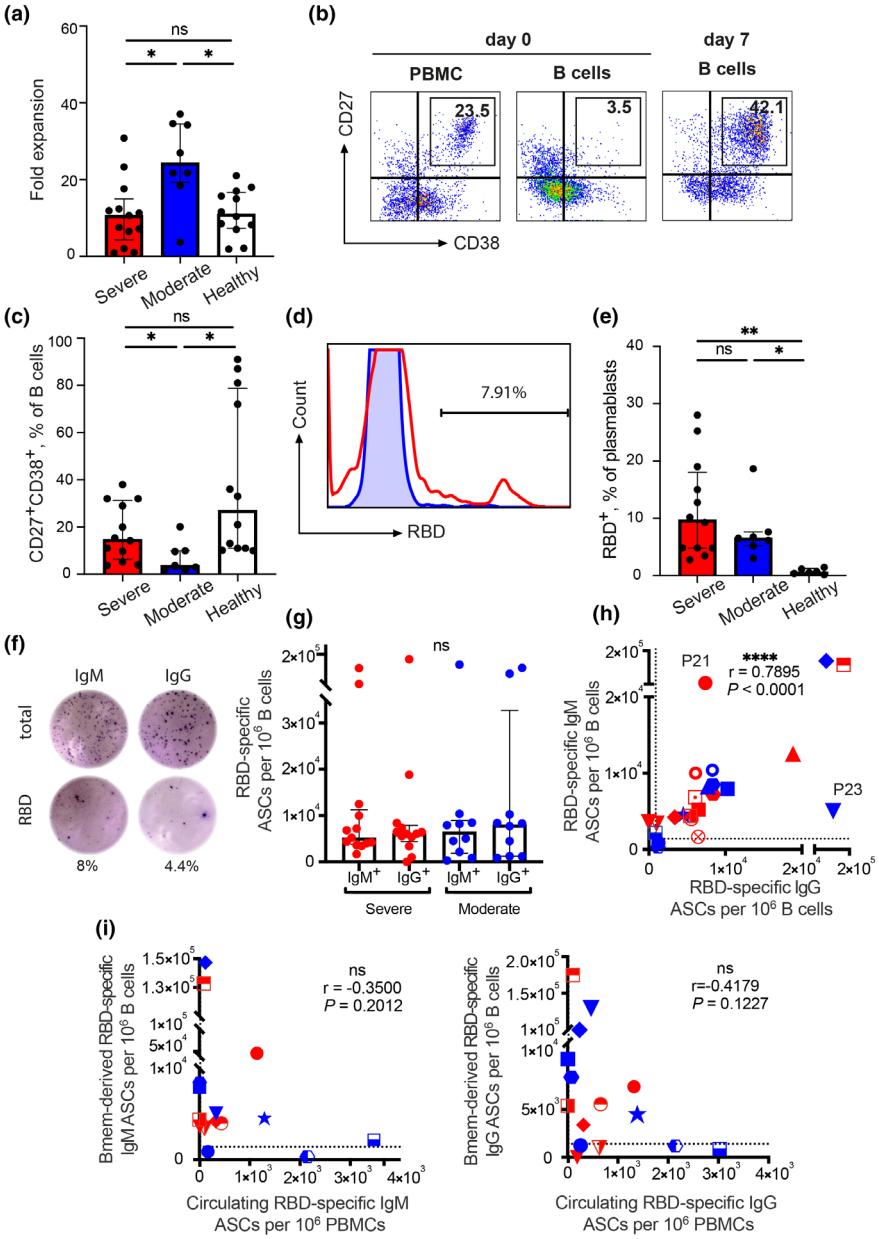


**Figure 4.** CD40L/IL-21-induced cell expansion and activation and ASC generation in purified B cells. **(a)** Fold expansion after 7 days of IL-21/CD40L stimulation of B cells from HDs (n = 12), and moderate (n = 10) and severe (n = 13) COVID-19 cases. **(b)** Representative flow plots depicting the generation of stimulated B cells *in vitro*. Fresh PBMCs (left), immunomagnetically purified B cells (middle), and B cells after stimulation for 7 days (right) were analysed using flow cytometry. **(c)** *In vitro* generation of $CD27^+CD38^+$ B cells after 7 days of IL-21/CD40L stimulation in HDs and patients with moderate and severe COVID-19. **(d)** Representative flow plot of $RBD^+CD27^+CD38^+$ B cells after IL-21/CD40L stimulation for 7 days; 500 000 B-cell events were acquired. **(e)** *In vitro* generation of $RBD^+CD27^+CD38^+$ B cells after IL-21/CD40L stimulation for 7 days. **(f)** Representative ELISpot showing RBD-specific Bmem cell-derived ASCs. Purified B cells were stimulated with IL-21/CD40L for 7 days and then incubated on ELISpot plates for 16 h to detect cells secreting total (top row) or RBD-specific (bottom row) IgMs (right column) or IgGs (left column). The percentages indicated beside the wells represent the frequencies of antigen-specific ASCs relative to the total number of IgMs or IgGs. The wells shown contained $10^4$ purified B cells obtained from patients with COVID-19. **(g)** RBD-specific Bmem cell-derived ASCs per $10^6$ PBMCs in patients with severe (n = 13) and moderate (n = 10) COVID-19. **(h)** Scatter plot of RBD-specific IgG vs. IgM ASCs after 7 days of IL-21/CD40L stimulation. The dotted lines indicate the threshold for a positive RBD-specific ASC response (220 for IgG spots and 1400 for IgM spots per $10^6$ B cells). **(i)** Scatter plot of circulating vs. Bmem cell-derived RBD-specific IgM (left panel) or IgG (right panel) ASCs. Data are presented as median ± IQR. Asterisks indicate significant difference between groups determined using the Kruskal–Wallis test, $*P < 0.05$, $**P < 0.01$, $****P < 0.0001$, ns = not significant. ASC, antibody-secreting cell; Bmem cell, memory B cell; HD, healthy donor; RBD, receptor-binding domain.

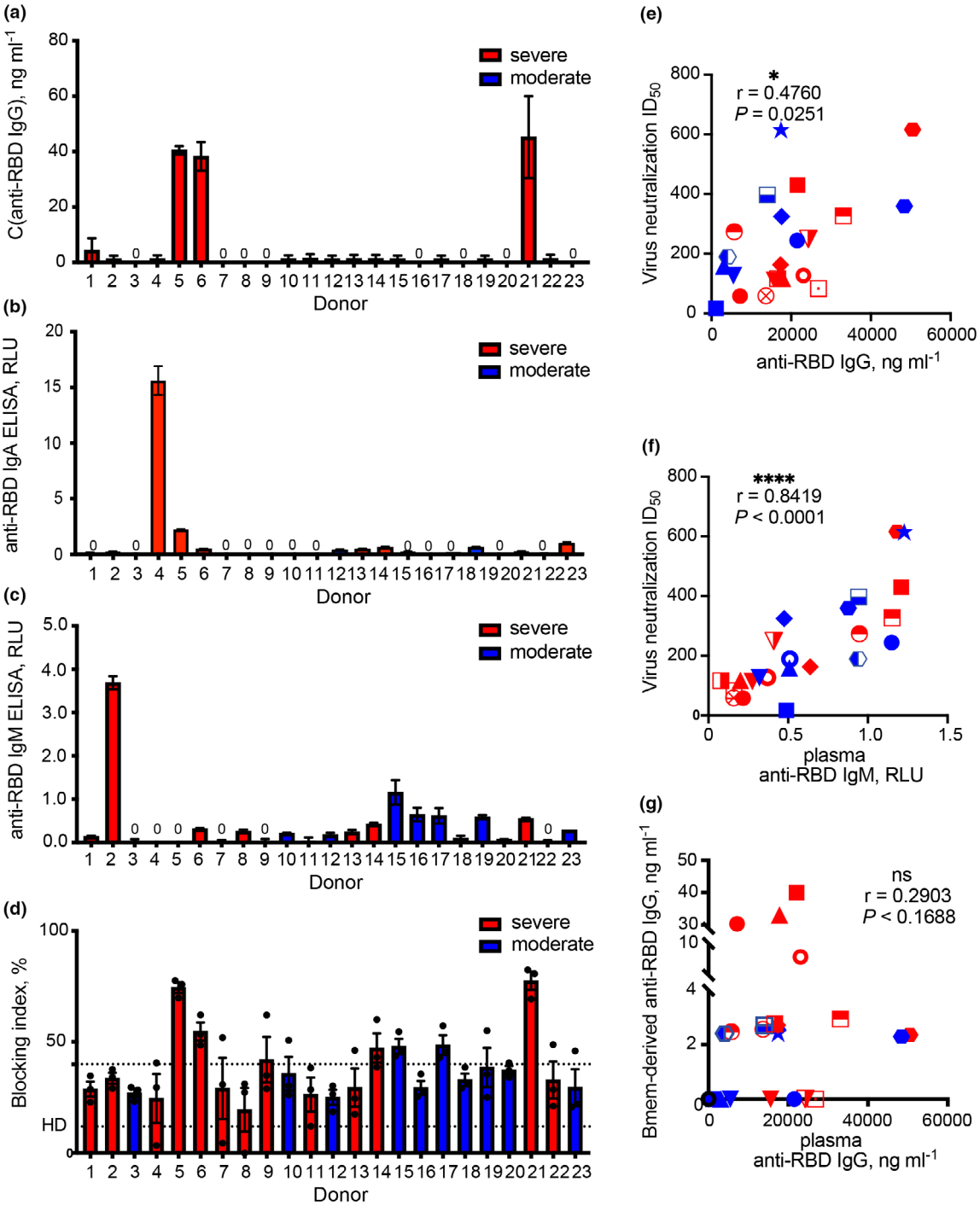


**Figure 5.** Activity of anti-SARS-CoV-2 antibodies derived from cultures of CD40L/IL-21-stimulated B cells. **(a–c)** Production of RBD-specific IgGs **(a)**, IgAs **(b)** or IgMs **(c)** in cultures of IL-21/CD40L-stimulated B cells obtained from different patients with COVID-19 evaluated using ELISA. The dotted line indicates the mean level of total IgGs observed in the HD group. The results of three separate experiments are presented for all patients. **(d)** Antibody-mediated neutralisation assay of HIV-1-based virions pseudotyped with spike proteins of SARS-CoV-2. Supernatants from IL-21/CD40L-stimulated B-cell cultures were used as a source of antibodies. The bottom dotted line indicates the mean level of virus neutralisation observed in the HD group. The upper dotted line indicates a cut-off value for the virus neutralisation test. The results of three separate experiments are presented for all patients. (e-f) Spearman's correlation between virus neutralisation half-maximal inhibitory plasma dilution ($ID_{50}$) values and the levels of plasma anti-RBD IgG **(e)** or IgM **(f)**. **(g)** Scatter plot of Bmem cell-derived vs. plasma anti-RBD IgG. C, concentration; HD, healthy donor; ID, inhibitory dilution; OD, optical density; RBD, receptor-binding domain

The SARS-CoV-2-pseudotyped virus-like particles (VLPs) infected ACE2-expressing HEK293T cells, and approximately 50% of the target cells showed a strong GFP signal (Supplementary figure 8). The control human monoclonal antibody 34B12 efficiently prevented the entry of pseudotyped VLPs into target cells, and in this case, $GFP^+$ cells were not formed. Samples from stimulated B-cell cultures were directly used in the neutralisation assay without dilution. To distinguish between positive and negative samples, a cut-off value for virus neutralisation was set at 40%. It was found that supernatants from 3 of the 23 samples (obtained from patients P5, P6 and P21) exhibited strong reactivity in pseudotype HIV-1 neutralisation assays (Figure 5d). In addition, supernatants from three other samples (derived from patients P14, P15 and P17) exhibited neutralisation at a value marginally above the cut-off value. Notably, the samples (derived from P5, P6 and P21) that exhibited the highest activity in the neutralisation test also had the highest concentration of anti-RBD IgG, while they did not have the highest concentration of anti-RBD IgM. This suggests that RBD-specific IgGs, and may be IgAs, contributed to the virus neutralisation activity of supernatants derived from the Bmem cell cultures. Therefore, patient Bmem cell-derived antibodies displayed highly heterogeneous yet correlated RBD-binding and neutralisation activities. Our results indicated that only a small percentage of patients with acute COVID-19 possessed Bmem cells that could produce antibodies that could directly neutralise the epitopes of SARS-CoV-2.

Contrary to the pattern of anti-RBD activity observed in cell culture supernatants, almost all plasma samples (except that derived from P20) showed high levels of RBD-specific IgG and IgM, which correlated with the virus-neutralising capacity (Spearman's $r = 0.48$, $P = 0.025$ for IgG; Figure 5e; Spearman's $r = 0.84$, $P = 0.0001$ for IgM; Figure 5f). No correlation was observed between the plasma and Bmem cell-derived RBD-specific IgGs (Figure 5g). Only in samples collected from patients P5, P6 and P21, a correspondence was noted between the plasma and culture supernatant-derived RBD-specific IgGs (Figure 5g). These results indicated that the plasma and Bmem cell-derived RBD-specific antibodies originated from different and indirectly connected B-cell subsets, which had different BCR repertoires.

## DISCUSSION

Humoral immunity is a function of two B-cell subsets: Bmem cells and plasma cells. Circulating plasmablasts are the precursors of plasma cells. Therefore, the induction of both plasmablasts and Bmem cells is a prerequisite for the generation of humoral immune memory. In this study, the B-cell response during the acute phase of SARS-CoV-2 infection was analysed using three assays: (i) determination of RBD-binding plasmablast frequency by RBD-PE staining, (ii) evaluation of circulating RBD-specific ASCs using an ELISpot assay, and (iii) characterisation of Bmem cells by ELISpot analysis after IL-21/CD40L stimulation.

It is interesting to compare the parameters of SARS-CoV-2 response observed in the current study with the data available on humoral immunity against other viral infections. A transient increase in the plasmablast frequency is a characteristic feature of several viral and bacterial infections.[21,22] For example, the frequency of plasmablasts can increase from 10 to 50% of the total B-cell population during infection by Dengue virus,[23] Zika virus[24] and Ebola virus.[25] An expansion of the plasmablast population has also been noted after vaccination for influenza, hepatitis and other diseases.[26] The increase in the number of plasmablasts observed herein is also consistent with the recently reported findings on patients with COVID-19.[27–29]

Virus-specific lymphocytes are of particular interest. The most direct method for the enumeration of antigen-specific B cells involves the binding of a fluorescently labelled antigen. The staining of PBMCs derived from patients with acute disease or convalescent patients using fluorochrome-labelled RBD or S trimer showed the presence of 0.075–1.86% of antigen-specific Bmem cells in the total B-cell population.[4,5,11,12,30–32] The percentage of antigen-positive cells varied widely depending on the number of days after symptom onset as well as the individual characteristics of donors. RBD-specific cells primarily include $IgM^+IgD^+$ non-class-switched Bmem cells, and to a lesser extent, class-switched $IgG^+$ Bmem cells.[11] Isolated antigen-specific Bmem cells were used as a source of Ig genes for the subsequent isolation of virus-neutralising antibodies; however, these were not used for the assessment of the Bmem cell population. It has been reported that at 3 months post-symptom onset, patients who have recovered

from COVID-19 develop a distinct population of RBD-specific cells with a phenotype of typical resting Bmem cells ($IgG^+CD27^+CD21^+T\text{-}bet^{lo}$).[30,33]

For the evaluation of SARS-CoV-2-specific B cells along with the analysis of RBD-binding cells, we performed additional ELISpot assays. The frequencies of RBD-specific circulating ASCs in patients with COVID-19 ranged from 200 to 4000 ASCs per $10^6$ PBMCs, which corresponded to the level of virus-specific ASCs observed during other viral infections in terms of the order of magnitude. For example, the frequency of virus-specific ASCs is approximately 200 per $10^6$ PBMCs during acute respiratory syncytial virus infection[34] or after experimental influenza infection,[35] whereas it is about 1000 ASCs during natural influenza infection.[36] The frequency of virus-specific ASCs detected during acute secondary Dengue virus infection is significantly high, with 200 000 or more ASCs detected per $10^6$ PBMCs.[37,38]

Usually, virus-specific ASCs constitute the majority of total Ig ASCs. The frequency of Zika virus-specific plasmablasts relative to the total number of IgG ASCs reaches up to 25%.[24] After immunisation to influenza virus, more than 82% of the IgG ASCs detected are found to be antigen-specific.[39] Similarly, in our study, the percentage of RBD-specific ASCs was high, and in certain cases, it reached up to 80%. Notably, for the detection of SARS-CoV-2-specific cells in the ELISpot assay, we used recombinant RBD, which constitutes only a part of the viral proteome. Therefore, the total SARS-CoV-2-specific ASC response is expected to be more significant.

The induction of B-cell immunity can be evaluated by tracking the dynamics of plasmablast response and the generation of Bmem cells. The dynamics of total and antigen-specific plasmablast generation have been tracked in a human influenza challenge model.[35] After vaccination, the levels of antigen-specific ASCs in the peripheral blood samples peaked approximately at day 7 post-immunisation,[40] whereas during natural viral infection, plasmablasts were found to circulate in the blood for a longer period of time depending on the severity of the disease.[25] In line with this observation, in most of the cases in our study, the plasmablast frequency declined to the baseline level in 20 days, while in some critically ill patients, significant plasmablast frequencies (>15% of total B cells) were observed for up to 70 days after disease onset. Since the plasmablast population is transient, maintaining high plasmablast levels is only possible through recruitment from new naïve B cells, plasmablast self-renewal, or re-stimulation of Bmem cells. Continuous plasmablast generation has been noted during the infection period in patients infected with influenza virus.[36]

In addition to the circulating ASC response, we clearly detected a Bmem cell response during the acute phase of SARS-CoV-2 infection. The proportion of RBD-specific IgM or IgG Bmem cells in patients with COVID-19 ranged from 4000 to 200 000 ASCs per $10^6$ cells in the total B-cell population. In other viral infections, comparable number of Bmem cells has been observed.[35,41–43]

Notably, in 5 of 23 patients, the frequency of RBD-specific Bmem cells was considerably low and close to the baseline levels detected in uninfected individuals. This suggests that Bmem cells may not have formed in these individuals when they were examined. However, Bmem cells can be generated quite early during acute viral infection. In a human influenza challenge model, Bmem cells have been shown to appear by the third day of infection, and their levels peaked on day 28.[35] According to another theory, these patients could be low- or non-responders. Possibly, Bmem cell non-responsiveness may be associated with the age-related downregulation of the IL-21/IL-21R signalling axis.[44]

According to the classical pathway of differentiation, after antigen-induced activation, naïve B cells differentiate into plasmablasts, Bmem cells and short- or long-lived plasma cells.[21] Using the data obtained, we could evaluate the relationship between plasmablast and Bmem cell frequencies during the course of SARS-CoV-2 infection. We observed no correlation between the frequencies of circulating and Bmem-derived ASCs. In addition, there was no correlation between the levels of virus-specific antibodies in the plasma and antibodies secreted by *in vitro*-stimulated Bmem cells. These results suggest that plasmablasts and Bmem cells generated during SARS-CoV-2 infection do not belong to directly related subsets. Plasmablast and classical Bmem cell development has been suggested to occur *via* separate pathways in cases of Dengue virus reinfection.[45] A high-dimensional flow cytometry analysis showed that in patients with severe COVID-19, the massive plasmablast response is associated with extrafollicular pathway of activation.[46] This is in good agreement with the absence of germinal centres in patients with severe COVID-19.[47] Based on our observation that there was no correlation between the plasmablast and Bmem cell responses,

we suggested that Bmem cells, in contrast to plasmablasts, mainly developed in the traditional follicular pathway. This can be clarified by comparing the BCR repertoires of plasmablasts and Bmem cells.

In certain critical cases, SARS-CoV-2 infection lasted for 2 months or more. This leads to chances of the generation of atypical Bmem cells, which are detected in certain chronic viral infections.[48] In line with this, a significant increase in the proportion of $CD21^{-}CD27^{-}$ cells has been observed in patients with COVID-19.[28]

In recent times, several laboratories have generated SARS-CoV-2-specific human monoclonal antibodies.[12,49–51] This method is rather time consuming, as it requires Bmem cell sorting, single-cell Ig sequencing, and subsequent antibody expression. It has been noted that potent virus-neutralising antibodies may be generated using samples from no more than 30% of convalescent individuals. Using IL-21/CD40L-induced *in vitro* activation of Bmem cells, it is possible to pre-screen convalescent individuals in whom the most potent virus-neutralising antibodies are generated,[32] and this appears to be the optimal approach.

In this study, we demonstrated that Bmem cells are generated in most cases of acute SARS-CoV-2 infection. After activation, they are capable of secreting RBD-specific and virus-neutralising antibodies. Therefore, during acute SARS-CoV-2 infection, the B-cell memory formed can be considered adequate. However, it is unclear whether this Bmem cell-mediated immunity is long lasting. Our results can serve as a basis for further investigation on the longevity of SARS-CoV-2-specific B-cell memory. We intend to characterise the Bmem cell response at multiple time points post-infection. The extension of such studies to the post-infection period will be important to assess the likelihood of SARS-CoV-2 reinfection and evaluate the efficacy of the SARS-CoV-2 vaccines currently under development.

# METHODS

## Participants and ethics

A total of 72 patients with COVID-19 were enrolled in a study performed at the Federal Research Clinical Center of the Federal Medical-Biological Agency of Russia (FRCC). For all patients, SARS-CoV-2 infection was confirmed by RT-PCR of the oropharyngeal and nasopharyngeal swabs. Samples were collected in the acute phase of the disease at a late time point (days 8–65) from the onset of the disease. As a reference, we used an age-matched healthy donor (HD) cohort that tested negative in the RT-PCR and for COVID-19 antibodies in ELISA ($n = 10$). Study protocol was reviewed and approved by the Medical Ethical Committee of FRCC (#4-2020 April 28, 2020). Written informed consent was obtained from all study participants before performing any study procedures.

## Processing of blood samples

Peripheral venous blood was collected in heparinised vacutainer tubes. PBMCs were isolated by density gradient centrifugation. Plasma samples were stored at −80°C. B cells were purified from PBMCs by negative selection using the Dynabeads Untouched human B cells kit (Thermo Fisher Scientific, Carlsbad, CA, USA). Due to the peculiarity of the kit used by us for the immunomagnetic isolation, the purified B cells were completely deprived of plasmablasts. For *in vitro* differentiation of B cells, cells were cultured in DMEM medium supplemented with 10% foetal bovine serum, 24 μg $mL^{-1}$ of gentamicin, 1 mM sodium pyruvate, 10 mM HEPES (all Paneko, Moscow, Russia) and 25 ng $mL^{-1}$ interleukin-21 (IL-21; PeproTech, Rocky Hill, CT, USA) in the presence of mitomycin-treated feeder A549 cells stably expressing CD40L (A549-CD40L, $1 \times 10^5$ cells/well) according to the method published by Kwakkenboss *et al.*[19]. Stimulated B cells were harvested after 7 days of incubation at 37°C in 5% $CO_2$. A part of B cells was used in ELISpot assay, and the remaining cells were stained for flow cytometry analysis. Supernatants from each well were also collected for measuring secreted antibodies in ELISA or virus neutralisation assay.

## Flow cytometry

Flow cytometry experiments were performed on freshly isolated PBMCs or B cells after IL-21/CD40L stimulation using a CytoFLEX S flow cytometer (Beckman Coulter, Krefeld, Germany). The following antibodies were used: CD3 FITC (clone TB3), CD16 FITC (clone LNK16), CD19 PE (clone LT19), CD27 PECy5.5 (clone LT27), CD38 PECy7 (clone LT38), anti-human IgG HRP (clone CH1), anti-human IgM HRP (clone MA2) were produced earlier in our laboratory [52,53]; CD14 (clone MEM-15) from Exbio (Praha, Czech Republic); and anti-human IgG APC (clone M1310G05) and anti-human IgM APC-Fire750 (clone MHM-88) from BioLegend (San Diego, CA, USA).

Recombinant RBD domain (residues 319–541) was earlier produced in the laboratory of G. Efimov (National Research Center for Hematology, Moscow, Russia). His-tagged RBD was expressed using the Expi293 Expression System (Thermo Fisher Scientific) and purified from cell culture supernatant using affinity chromatography on Ni-NTA agarose resin (QIAGEN, Hilden, Germany). Betv1 (kind gift from R. Valenta, Medical University of Vienna, Austria) was used as irrelevant protein for negative control. RBD and Betv1 were conjugated to PE or APC (Agilent Technologies, Palo Alto, CA) using copper-free click chemistry reaction.[54] These probes were used for surface B-cell staining.

For detection of plasmablasts, PBMCs were stained with CD19 PE, CD27 PECy5.5, CD38 PECy7 and a dump channel mix containing FITC-labelled anti-human CD3, CD14 and

CD16. Plasmablasts, naïve B cells and Bmem were sorted with a Sony SH800S cell sorter (Sony Biotechnology, San Jose, CA, USA). FlowJo Software (version 10.6.1., Tree Star, Ashland, OR, USA) was used for analysing data.

## ELISA

The level of antibodies against SARS-CoV-2 RBD was measured using ELISA Quantitation Kit (Xema Co., Moscow, Russia). Plasma samples were 2-fold serially diluted from 1:40 to 1:5000 in blocking buffer, and a volume of 100 μL of each diluted sample was added to each microplate well in triplicate. An anti-SARS-CoV-2 RBD human monoclonal antibody 34B12 (a kind gift from A Taranin, Institute of Molecular and Cellular Biology, Novosibirsk, Russia) was used as positive control and calibration standard for determination of RBD-specific IgG concentration.

## ELISpot assay

For the detection of IgM and IgG RBD-specific ASCs, an in-house ELISpot assay was developed. Sterile clear 96-well Multiscreen HTS Filter Plates with 0.45 μm pore size, hydrophobic polyvinylidene difluoride (PVDF) membrane (Merck Millipore Ltd, Cork, Ireland) were stripped with 70% and coated with 100 μL/well of recombinant RBD domain at 10 μg $mL^{-1}$ at 4°C overnight. To capture the total Ig ASC response, wells were coated with 10 μg/well of rabbit anti-human IgG or IgM antibody (R&D Systems, Minneapolis, MN, USA). Fresh PBMCs or stimulated B cells were plated at 250000–2500000 cells per well in duplicate and incubated for 16 h at 37°C, 5% $CO_2$. The cells were thoroughly removed with washing buffer (0.05% Tween 20 in PBS).

After the addition of detection biotinylated rabbit anti-human IgG or biotinylated rabbit anti-human IgM (R&D Systems), plates were incubated for 16 h. After washing three times with 0.05% Tween-20/PBS, Streptavidin-alkaline phosphatase (R&D Systems) was added at a dilution of 1:60 and plates were further incubated for 2 h at RT. After a few washings, the colorimetric reaction was developed by adding substrate reagent from B Cell ELISpot Development Module Human IgG or IgM (R&B Systems) until distinct spots emerged. The reaction was stopped by gently rinsing the plate with tap water. ELISpot images were captured using CTL ImmunoSpot® Analyzer (CTL, Shaker Heights, OH, USA). Spot number was counted using ImmunoSpot® Software. The percentage of RBD-specific ASCs was calculated by dividing the number of RBD-specific by the total number of IgM- or IgG-secreting cells. Wells coated with irrelevant protein served as negative controls.

## Pseudotyped virus neutralisation assay

To generate SARS-CoV-2 pseudotyped HIV-1-based virus-like particles, we used 3 plasmids: HIV-1 packaging plasmid pCMVΔ8.2R (Addgene, Teddington, UK), reporter pUCHR-GFP plasmid[55] and pCG1-SARS-S plasmid encoding the full-length SARS-CoV-2 spike protein (kind gift from Stefan Pöhlmann, Leibniz Institute for Primate Research, Germany).[56] The HEK293T cells were plated 18–24 h before transfection at $3.6 \times 10^6$ cells per 10-cm petri dish. Plasmids were mixed (pCG1-SARS-S 2.7 μg; pCMVΔ8.2R 8.7 μg; pUCHR-GFP 13.2 μg) and transfected into HEK293T cells using calcium phosphate-based protocol. After 6 h, the culture medium was replaced, and cells were grown for another 48 h. Supernatant from the 10-cm dish with transfected HEK293T cells was harvested and clarified through a 0.45-μm pore size filter. Virus-like particles (VLPs) in the supernatant were concentrated by centrifugation at 30000 *g* for 2.5 h and resuspended in 0.3 mL of fresh RPMI culture medium, aliquoted and cryopreserved. VLP were used at a 1: 4 dilution that provided infection in 50% of the target cells.

To generate SARS-CoV-2 permissive cell line, HEK293T cells were stably transduced with the human ACE2 receptor. The sequence coding for ACE2 was subcloned from the pCG1-hACE2 plasmid (a gift from Prof. Stefan Pöhlmann) into the lentiviral vector pUCHR. HEK293T cells were co-transfected with pCMVΔ8.2R, pUCHR-hACE2, and pCMV-VSVG to generate VLPs, which were used to infect HEK293T cells at ~30% MOI. Three days post-infection, HEK293T cells were stained with the rabbit anti-hACE2 polyclonal Ab (Cloud-Clone Corp, Katy, TX, USA) plus corresponding secondary Ab, and hACE2-positive cells were isolated using several rounds of sorting by flow cytometry. These cells have a high hACE2 expression and were hereafter referred to as 293-ACE2.

For the neutralisation assay, 20 μL of serially diluted antibodies was incubated with 10 μL of pseudotyped viral particles and added to 293-ACE2 cells plated at $5 \times 10^3$ cells/well in 10 μL of medium in 96-well plates. Cells were then cultured for 48 h. After that, cells were resuspended and the percentage of $GFP^+$ cells was enumerated using CytoFLEX S flow cytometer. Neutralisation half-maximal inhibitory plasma dilution ($ID_{50}$) values were determined using a normalised nonlinear regression with GraphPad Prism software (Sigmoidal, 4PL).

## Statistical analysis

The Kruskal–Wallis H test was used for comparison between multiple groups. $P < 0.05$ was considered statistically significant. Non-parametric Spearman correlations analyses were used to determine associations between analysed parameters.

All statistical analyses were carried out using GraphPad Prism (version 8.4.3 GraphPad Software, La Jolla California USA). Data are indicated by medians and interquartile ranges (IQR). Non-parametric LOESS (LOcal regrESSion) was used for smoothing.

# ACKNOWLEDGMENTS

This work is supported by the Russian Scientific Foundation (Project 19-15-00331). The authors thank all donors who volunteered for our study., and We thank our colleagues Elina Zheremyan, Ekaterina Astakhova and Julia Vasiljeva for their kind help with experiments; Alexander Taranin, Yuri Lebedin and Rudolf Valenta for providing reagents; and Alexander Kovalchuk, Rudolf Valenta and Alexander Taranin for helpful discussion and critical reading of the manuscript. The subcloning and sequencing of ACE2 and

SARS-Cov2-S protein expression plasmids were performed using the equipment of the Institute of Gene Biology RAS facilities supported by the Ministry of Science and Higher Education of the Russian Federation.

## AUTHOR CONTRIBUTION

**Maria G Byazrova:** Data curation; Formal analysis; Investigation; Methodology; Software; Supervision; Validation; Visualization. **Gaukhar M. Yusubalieva:** Data curation; Investigation; Methodology; Resources. **Anna B. Spiridonova :** Investigation; Methodology. **Grigory A. Efimov:** Methodology; Resources; Writing-original draft; Writing-review & editing. **Dmitriy Mazurov:** Methodology; Resources; Writing-review & editing. **Konstantin O. Baranov:** Investigation; Methodology. **Vladimir P. Baklaushev:** Conceptualization; Project administration; Resources; Supervision; Writing-original draft. **Alexander V Filatov:** Conceptualization; Funding acquisition; Project administration; Resources; Supervision; Validation; Writing-original draft; Writing-review & editing.

## CONFLICT OF INTEREST

The authors declare no conflict of interest.

## REFERENCES

1. Shah VK, Firmal P, Alam A, Ganguly D, Chattopadhyay S. Overview of immune response during SARS-CoV-2 infection: lessons from the past. *Front Immunol* 2020; **11**: 1949.
2. Moderbacher CR, Ramirez SI, Dan JM *et al*. Antigen-specific adaptive immunity to SARS-CoV-2 in acute COVID-19 and associations with age and disease severity. *Cell* 2020; **183**: 996–1012.
3. Walls AC, Park Y-J, Tortorici MA, Wall A, McGuire AT, Veesler D. Structure, Function, and Antigenicity of the SARS-CoV-2 Spike Glycoprotein. *Cell* 2020; **181**: 281–292.
4. Ju B, Zhang QI, Ge J *et al*. Human neutralizing antibodies elicited by SARS-CoV-2 infection. *Nature* 2020; **584**: 115–119.
5. Robbiani DF, Gaebler C, Muecksch F *et al*. Convergent antibody responses to SARS-CoV-2 in convalescent individuals. *Nature* 2020; **584**: 437–442.
6. Rogers TF, Zhao F, Huang D *et al*. Isolation of potent SARS-CoV-2 neutralizing antibodies and protection from disease in a small animal model. *Science* 2020; **369** (6506): 956–963.
7. Lin Q, Zhu L, Ni Z, Meng H, You L. Duration of serum neutralizing antibodies for SARS-CoV-2: Lessons from SARS-CoV infection. *J Microbiol Immunol Infect* 2020; **53**: 821–822.
8. Cao W-C, Liu W, Zhang P-H, Zhang F, Richardus JH. Disappearance of antibodies to SARS-associated coronavirus after recovery. *N Engl J Med* 2007; **357**: 1162–1163.
9. Tang F, Quan Y, Xin Z-T *et al*. Lack of peripheral memory B cell responses in recovered patients with severe acute respiratory syndrome: a six-year follow-up study. *J Immunol* 2011; **186**: 7264–7268.
10. Le Bert N, Tan AT, Kunasegaran K *et al*. SARS-CoV-2-specific T cell immunity in cases of COVID-19 and SARS, and uninfected controls. *Nature* 2020; **584**: 457–462.
11. Seydoux E, Homad LJ, MacCamy AJ *et al*. Analysis of a SARS-CoV-2-infected individual reveals development of potent neutralizing antibodies with limited somatic mutation. *Immunity* 2020; **53**(98–105): e5.
12. Wan J, Xing S, Ding L *et al*. Human-IgG-neutralizing monoclonal antibodies block the SARS-CoV-2 infection. *Cell Rep* 2020; **32**: 107918.
13. Hartley GE, Edwards ESJ, Aui PM *et al*. Rapid generation of durable B cell memory to SARS-CoV-2 spike and nucleocapsid proteins in COVID-19 and convalescence. *Sci Immunol* 2020; **11**: e01991-20. https://doi.org/10.1126/sciimmunol.abf8891
14. Dan JM, Mateus J, Kato Y *et al*. Immunological memory to SARS-CoV-2 assessed for greater than six months after infection. *bioRxiv* 2015; **2020**(2011): 383323.
15. Boonyaratanakornkit J, Taylor JJ. Techniques to study antigen-specific B cell responses. *Front Immunol* 2019; **10**: 1694.
16. Kwakkenbos MJ, Bakker AQ, van Helden PM *et al*. Genetic manipulation of B cells for the isolation of rare therapeutic antibodies from the human repertoire. *Methods* 2014; **65**: 38–43.
17. Blanc P, Moro-Sibilot L, Barthly L *et al*. Mature IgM-expressing plasma cells sense antigen and develop competence for cytokine production upon antigenic challenge. *Nat Commun* 2016; **7**: 13600.
18. Henn AD, Rebhahn J, Brown MA *et al*. Modulation of single-cell IgG secretion frequency and rates in human memory B cells by CpG DNA, CD40L, IL-21, and cell division. *J Immunol* 2009; **183**: 3177–3187.
19. Kwakkenbos MJ, Diehl SA, Yasuda E *et al*. Generation of stable monoclonal antibody–producing B cell receptor–positive human memory B cells by genetic programming. *Nat Med* 2010; **16**: 123–128.
20. Fournier EM, Velez M-G, Leahy K *et al*. Dual-reactive B cells are autoreactive and highly enriched in the plasmablast and memory B cell subsets of autoimmune mice. *J Exp Med* 2012; **209**: 1797–1812.
21. Fink K. Origin and function of circulating plasmablasts during acute viral infections. *Front Immunol* 2012; **3**: 78.
22. Lu DR, Tan Y-C, Kongpachith S *et al*. Identifying functional anti-*Staphylococcus aureus* antibodies by sequencing antibody repertoires of patient plasmablasts. *Clin Immunol* 2014; **152**: 77–89.
23. Balakrishnan T, Bela-Ong DB, Toh YX *et al*. Dengue virus activates polyreactive, natural IgG B cells after primary and secondary infection. *PLoS One* 2011; **6**: e29430.
24. Bhaumik S, Priyamvada L, Kauffman R *et al*. Pre-existing Dengue immunity drives a DENV-biased plasmablast response in ZIKV-onfected patient. *Viruses* 2018; **11**: 19.
25. McElroy AK, Akondy RS, Davis CW *et al*. Human Ebola virus infection results in substantial immune activation. *Proc Natl Acad Sci USA* 2015; **112**: 4719–4724.
26. Qian Y, Wei C, Eun-Hyung Lee F *et al*. Elucidation of seventeen human peripheral blood B-cell subsets and quantification of the tetanus response using a density-based method for the automated identification of cell populations in multidimensional flow cytometry data. *Cytometry* 2010; **78B**: S69–S82.
27. De Biasi S, Lo Tartaro D, Meschiari M *et al*. Expansion of plasmablasts and loss of memory B cells in peripheral blood from COVID-19 patients with pneumonia. *Eur J Immunol* 2020; **50**: 1283–1294.

28. Kuri-Cervantes L, Pampena MB, Meng W *et al*. Comprehensive mapping of immune perturbations associated with severe COVID-19. *Sci Immunol* 2020; **5**: eabd7114.
29. Mathew D, Giles JR, Baxter AE *et al*. Deep immune profiling of COVID-19 patients reveals distinct immunotypes with therapeutic implications. *Science* 2020; **369**: eabc8511.
30. Juno JA, Tan H-X, Lee WS *et al*. Humoral and circulating follicular helper T cell responses in recovered patients with COVID-19. *Nat Med* 2020; **26**: 1428–1434.
31. Liu L, Wang P, Nair MS *et al*. Potent neutralizing antibodies against multiple epitopes on SARS-CoV-2 spike. *Nature* 2020; **584**: 450–456.
32. Zost SJ, Gilchuk P, Chen RE *et al*. Rapid isolation and profiling of a diverse panel of human monoclonal antibodies targeting the SARS-CoV-2 spike protein. *Nat Med* 2020; **26**: 1422–1427.
33. Rodda LB, Netland J, Shehata L *et al*. Functional SARS-CoV-2-specific immune memory persists after mild COVID-19. *Cell* 2021; **184**:169–183.
34. Lee FE, Falsey AR, Halliley JL, Sanz I, Walsh EE. Circulating antibody-secreting cells during acute respiratory syncytial virus infection in adults. *J Infect Dis* 2010; **202**: 1659–1666.
35. Huang K-Y, Li C-F, Clutterbuck E *et al*. Virus-specific antibody secreting cell, memory B-cell, and sero-antibody responses in the human influenza challenge model. *J Infect Dis* 2014; **209**: 1354–1361.
36. Wrammert J, Koutsonanos D, Li G-M *et al*. Broadly cross-reactive antibodies dominate the human B cell response against 2009 pandemic H1N1 influenza virus infection. *J Exp Med* 2011; **208**: 181–193.
37. Priyamvada L, Cho A, Onlamoon N *et al*. B Cell Responses during secondary Dengue virus infection are dominated by highly cross-reactive, memory-derived plasmablasts. *J Virol* 2016; **90**: 5574–5585.
38. Wrammert J, Onlamoon N, Akondy RS *et al*. Rapid and massive virus-specific plasmablast responses during acute dengue virus infection in humans. *J Virol* 2012; **86**: 2911–2918.
39. Ellebedy AH, Jackson KJL, Kissick HT *et al*. Defining antigen-specific plasmablast and memory B cell subsets in human blood after viral infection or vaccination. *Nat Immunol* 2016; **17**: 1226–1234.
40. Halliley JL, Kyu S, Kobie JJ *et al*. Peak frequencies of circulating human influenza-specific antibody secreting cells correlate with serum antibody response after immunization. *Vaccine* 2010; **28**: 3582–3587.
41. Hartley GE, Edwards ESJ, Bosco JJ *et al*. Influenza-specific IgG1$^{+}$ memory B-cell numbers increase upon booster vaccination in healthy adults but not in patients with predominantly antibody deficiency. *Clin Transl Immunol* 2020; **9**: e1199.
42. Tian C, Chen Y, Liu Y *et al*. Use of ELISpot assay to study HBs-specific B cell responses in vaccinated and HBV infected humans. *Emerging Microbes & Infections* 2018; **7**: 1–10.
43. Walsh PN, Friedrich DP, Williams JA *et al*. Optimization and qualification of a memory B-cell ELISpot for the detection of vaccine-induced memory responses in HIV vaccine trials. *J Immunol Methods* 2013; **394**: 84–93.
44. Pallikkuth S, Pilakka Kanthikeel S, Silva SY, Fischl M, Pahwa R, Pahwa S. Upregulation of IL-21 receptor on B cells and IL-21 secretion distinguishes novel 2009 H1N1 vaccine responders from nonresponders among HIV-infected persons on combination antiretroviral therapy. *J Immunol* 2011; **186**: 6173–6181.
45. Appanna R, Kg S, Xu MH *et al*. Plasmablasts during acute Dengue infection represent a small subset of a broader virus-specific memory B cell pool. *EBioMedicine* 2016; **12**: 178–188.
46. Woodruff MC, Ramonell RP, Nguyen DC *et al*. Extrafollicular B cell responses correlate with neutralizing antibodies and morbidity in COVID-19. *Nat Immunol* 2020; **21**: 1506–1516.
47. Kaneko N, Kuo H-H, Boucau J *et al*. Loss of Bcl-6-expressing T follicular helper cells and germinal centers in COVID-19. *Cell* 2020; **183**: 143–157.
48. Portugal S, Obeng-Adjei N, Moir S, Crompton PD, Pierce SK. Atypical memory B cells in human chronic infectious diseases: an interim report. *Cell Immunol* 2017; **321**: 18–25.
49. Pinto D, Park Y-J, Beltramello M *et al*. Cross-neutralization of SARS-CoV-2 by a human monoclonal SARS-CoV antibody. *Nature* 2020; **583**: 290–295.
50. Tai W, Zhang X, He Y, Jiang S, Du L. Identification of SARS-CoV RBD-targeting monoclonal antibodies with cross-reactive or neutralizing activity against SARS-CoV-2. *Antiviral Res* 2020; **179**: 104820.
51. Wang C, Li W, Drabek D *et al*. A human monoclonal antibody blocking SARS-CoV-2 infection. *Nat Commun* 2020; **11**: 2251.
52. Filatov AV, Krotov GI, Zgoda VG, Volkov Y. Fluorescent immunoprecipitation analysis of cell surface proteins: A methodology compatible with mass-spectrometry. *J Immunol Meth* 2007; **319**: 21–33.
53. Khvastunova AN, Kuznetsova SA, Al-Radi LS *et al*. Anti-CD antibody microarray for human leukocyte morphology examination allows analyzing rare cell populations and suggesting preliminary diagnosis in leukemia. *Sci Rep* 2015; **5**: 12573.
54. Karver MR, Weissleder R, Hilderbrand SA. Synthesis and evaluation of a series of 1,2,4,5-tetrazines for bioorthogonal conjugation. *Bioconjugate Chem* 2011; **22**: 2263–2270.
55. Filatov A, Kruglova N, Meshkova T, Mazurov D. Lymphocyte phosphatase-associated phosphoprotein proteoforms analyzed using monoclonal antibodies. *Clin Trans Immunol* 2015; **4**: e44.
56. Hoffmann M, Kleine-Weber H, Schroeder S *et al*. SARS-CoV-2 cell entry depends on ACE2 and TMPRSS2 and is blocked by a clinically proven protease inhibitor. *Cell* 2020; **181**: 271–280.


## Supporting Information

Additional supporting information may be found online in the Supporting Information section at the end of the article.